Monthly Notices
of the
ROYAL ASTRONOMICAL SOCIETY
MNRAS **476,** 261–270 (2018) doi:10.1093/mnras/sty166

ASASSN-15no: the Supernova that plays hide-and-seek

S. Benetti,[1]★ L. Zampieri,[1] A. Pastorello,[1] E. Cappellaro,[1] M. L. Pumo,[1,2,3] N. Elias-Rosa,[1] P. Ochner,[1] G. Terreran,[1,4,5] L. Tomasella,[1] S. Taubenberger,[6,7] M. Turatto,[1] A. Morales-Garoffolo,[8] A. Harutyunyan[9] and L. Tartaglia[10,11]

[1]*INAF - Osservatorio Astronomico di Padova, Vicolo dell'Osservatorio 5, I-35122 Padova, Italy*
[2]*Universitá degli Studi di Catania, DIEEI and DFA, Via Santa Sofia 64, I-95123 Catania, Italy*
[3]*INFN-Laboratori Nazionali del Sud, Via Santa Sofia 62, I-95123 Catania, Italy*
[4]*Astrophysics Research Centre, School of Mathematics and Physics, Queen's University Belfast, Belfast BT7 1NN, UK*
[5]*Dipartimento di Fisica e Astronomia G. Galilei, Università di Padova, Vicolo dell'Osservatorio 3, I-35122, Padova, Italy*
[6]*Max-Planck-Institut für Astrophysik, Karl-Schwarzschild-Str. 1, D-85748 Garching, Germany*
[7]*European Southern Observatory, Karl-Schwarzschild-Str. 2, D-85748 Garching, Germany*
[8]*Department of Applied Physics, University of Cádiz, Campus of Puerto Real, E-11510 Cádiz, Spain*
[9]*INAF-Fundacion Galileo Galilei, Rambla Jose Ana Fernandez Perez 7, E-38712 Brena Baja, Spain*
[10]*Department of Astronomy and Steward Observatory, University of Arizona, 933 N Cherry Ave, Tucson, AZ 85719, USA*
[11]*Department of Physics, University of California, 1 Shields Ave, Davis, CA 95616, USA*

Accepted 2018 January 16. Received 2018 January 15; in original form 2017 November 28

ABSTRACT

We report the results of our follow-up campaign of the peculiar supernova ASASSN-15no, based on optical data covering ∼300 d of its evolution. Initially the spectra show a pure black-body continuum. After few days, the HeI λλ 5876 transition appears with a P-Cygni profile and an expansion velocity of about 8700 km s^{-1}. Fifty days after maximum, the spectrum shows signs typically seen in interacting supernovae. A broad (FWHM ∼ 8000 km s^{-1}) Hα becomes more prominent with time until ∼150 d after maximum and quickly declines later on. At these phases Hαstarts to show an intermediate component, which together with the blue pseudo-continuum are clues that the ejecta begin to interact with the circumstellar medium (CSM). The spectra at the latest phases look very similar to the nebular spectra of stripped-envelope SNe. The early part (the first 40 d after maximum) of the bolometric curve, which peaks at a luminosity intermediate between normal and superluminous supernovae, is well reproduced by a model in which the energy budget is essentially coming from ejecta recombination and ^{56}Ni decay. From the model, we infer a mass of the ejecta $M_{ej} = 2.6\,M_{\odot}$; an initial radius of the photosphere $R_0 = 2.1 \times 10^{14}$ cm; and an explosion energy $E_{expl} = 0.8 \times 10^{51}$ erg. A possible scenario involves a massive and extended H-poor shell lost by the progenitor star a few years before explosion. The shell is hit, heated, and accelerated by the supernova ejecta. The accelerated shell+ejecta rapidly dilutes, unveiling the unperturbed supernova spectrum below. The outer ejecta start to interact with a H-poor external CSM lost by the progenitor system about 9–90 yr before the explosion.

Key words: supernovae: general – supernovae: individual: ASASSN-15no.

1 INTRODUCTION

The final core-collapse (CC) of massive stars can produce a wide variety of events in terms of luminosity: luminous stripped-envelope (SE) supernovae (SNe) with M brighter than −18.5 mag (Mazzali et al. 2013), very weak SNe (e.g. fainter than ∼− 14 mag; Pastorello et al. 2004; Botticella et al. 2009; Spiro et al. 2014), or even failed SNe – when the star directly collapses on to a black hole without significant mass ejection (Heger et al. 2003; Adams et al. 2016; Reynolds et al. 2015).

Another class of very luminous transients, named superluminous supernovae (SLSNe, with $M < -21$ mag; Gal-Yam 2012) has been identified in recent years. These can occasionally reach a peak absolute magnitude exceeding −23.5 mag (Benetti et al. 2014; Dong et al. 2016). SLSNe sometimes show spectral signatures of H in their spectra (SLSNe-II), but in most cases their spectra are H-free (SLSNe-I) and they resemble those of SE SNe at late phases

★ E-mail: stefano.benetti@oapd.inaf.it

(Pastorello et al. 2010; Quimby et al. 2011). The mechanism that supports the tremendous energy released in SLSNe is not yet understood, but the most promising central engines are: (i) either a spinning-down magnetar (e.g. Kasen & Bildsten 2010; Woosley 2010; Inserra et al. 2013) or an accreting black hole (Dexter & Kasen 2013); (ii) the shock of the ejecta into a circumstellar shell (which can be H rich/poor) expelled by the progenitor star some time before the explosion (e.g. Blinnikov & Sorokina 2010; Chevalier & Irwin 2011; Wheeler et al. 2017); and (iii) the radioactive decay of a large amount of nickel produced in a pair-instability explosion (Gal-Yam et al. e.g. 2009, but see Moriya et al. 2010; Young et al. 2010; Nicholl et al. 2013).

The luminosity gap between normal and superluminous SNe is mostly populated by objects that show signs of interaction between fast expanding ejecta and a pre-existing circumstellar medium (CSM). The interacting system may be H rich, producing Type IIn SNe (Schlegel 1990; Filippenko 1997; Turatto et al. 2007) or He rich, producing the so-called Type Ibn SNe (Pastorello et al. 2016, and references therein).

The events populating this luminosity gaps can be very different as testified by the very recent supernova SN 2017dio (Kuncarayakti et al. 2017), showing early spectra typical of a SE-SN, whose ejecta soon collide with a H-rich CSM, showing for the first time the transition from a Type Ic to a bright Type IIn in just few weeks.

In these objects, the overall luminosity output include input from the ejected ^{56}Ni (which was shown to scale with the kinetic energy, Terreran et al. 2017), plus the conversion part of the kinetic energy of the ejecta into radiation in the interaction process, which depends on the physical properties of the CSM shell (such as density and radius). Assuming that the photosphere radiates as a blackbody, the luminosity increases with the radius, and/or with the photospheric temperature.

In the following sections, we will discuss the physical properties of ASASSN-15no, an object in the luminosity gap between normal SNe and SLSNe.

Our object was discovered by the ASAS-SN survey (Shappee et al. 2014) on 2015 August 3.26 ut (Holoien et al. 2015, 2017), and initially reported as an old Type Ic SN by Balam & Graham (2015). Actually, as we will show in this paper, the spectrum eventually developed broad H lines later on, that classifies the event as a Type II SN, caught at very early age. The redshift of the faint ($g = 18.57$ from SDSS DR10, Ahn et al. 2014), cigar shaped, host galaxy (SDSS J153825.20+465404.1) measured from unresolved emission lines in our Gran Telescopio Canarias (GTC) spectra (see Section 4), is $z = 0.03638 \pm 0.00008$. Assuming H_0=73 km s^{-1} Mpc^{-1} (Riess et al. 2016) and a flat cosmology with $\Omega_m = 0.31$ (Planck Collaboration XIII 2015), we obtain a luminosity distance $D_L = 153.5$ Mpc, hence a distance modulus of $\mu = 35.93$ mag. For the foreground Galactic extinction, we adopt $A(V) = 0.045$ mag (Schlafly & Finkbeiner 2011). Instead, since there is no evidence in the spectra of ASASSN-15nofor the presence of a narrow Na 1D absorption feature at the recessional velocity of the parent galaxy, we assume negligible host galaxy extinction.

2 OBSERVATIONS AND DATA REDUCTION

The follow-up campaign of ASASSN-15nowas carried out using several facilities, namely the 1.82 m Copernico Telescope equipped with AFOSC (located at Mount Ekar, Asiago, Italy); the 10.4 m GTC with OSIRIS; the 2.56 m Nordic Optical Telescope (NOT) with ALFOSC; Telescopio Nazionale Galileo (TNG) with Dolores

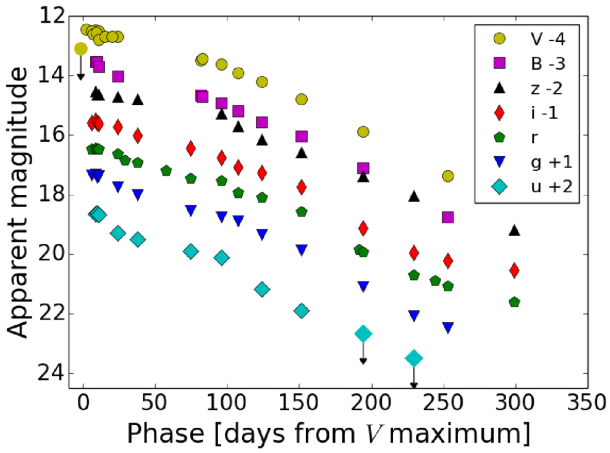

Figure 1. *BV* (Vega) and *ugriz* (AB mag) light curves of ASASSN-15no. The phase is in the observer's frame.

(these telescopes are located at the Observatorio del Roque de los Muchachos, La Palma, Spain); and the Telescopi Joan Orò with MEIA2 located at Mount Montsec, Catalonia, Spain. Additional *V* photometry has been supplied by the ASAS-SN telescopes.

Spectroscopic and photometric data were pre-processed in the standard manner (performing overscan, bias, and flat-field corrections) using IRAF[1] tasks. For the photometric measurements, the SNOOPY (Cappellaro 2014) package was used, which allowed us to extract the magnitude of the SN with the point-spread-function (PSF) fitting technique (Stetson 1987) for the *BVRI* frames, and the template subtraction technique for the *ugriz* frames (no deep template frames were available for BVRI bands). Indeed, *ugriz* template frames from the SDSS survey were obtained on 2012 June, 3 yr before the SN break out. The SN magnitudes were then calibrated with reference to the magnitudes of field stars retrieved from the SDSS catalog (DR9, Ahn et al. 2012). For the *BVRI* filters, we converted the SDSS catalog magnitudes into Johnson/Cousins, following Chonis & Gaskell (2008). The magnitudes of the Johnson/Cousins bands are thus given in the Vega system, while the SDSS ones are calibrated in the AB system.

Spectra of comparison lamps obtained with the same instrumental set-up were used for the wavelength calibration and standard stars observed in the same nights were used as reference for the flux calibration. The wavelength calibration was checked using night sky lines. The flux calibration was verified against the broad-band photometry, and a scaling factor was applied when necessary. Finally, we corrected the spectra of ASASSN-15nofor the Galactic foreground extinction and for the redshift of the host galaxy.

3 PHOTOMETRIC ANALYSIS

The *ugriz* and *BV* light curves are shown in Fig. 1, while the magnitudes in all bands (those shown in Fig. 1 plus *URI*) are reported in the online Tables 2 and 3.

The pre-discovery limit and discovery *V* magnitudes reported by Holoien et al. (2015) have been revised using deeper, higher quality reference images, and are shown in Fig. 1. No deep pre-discovery observations are available for BRI bands. This allows us to constrain the *V*-band maximum to 2015 August 1 ± 2 d (MJD=57235) and

[1] http://iraf.noao.edu/

Table 1. Log of the spectroscopic observations of ASASSN-15no.

Date	Rest phase	Instrumental set-up	Grism or grating	Spectral range (Å)	Resolution (Å)
20150806	+6	Ekar182+AFOSC	gm4	3400–8250	13.5
20150809	+9	Ekar182+AFOSC	gm4	3400–8250	13.5
20150810	+10	Ekar182+AFOSC	gm4/VPH6	3400–9280	14
20150811	+11	Ekar182+AFOSC	gm4	3400–8250	13.5
20150812	+12	Ekar182+AFOSC	gm4	3400–8250	13.5
20150817	+16	TNG+LRS	LRB/R	3230–9650	15
20150824	+23	NOT+ALFOSC	gm4	3450–9020	18
20150829	+28	GTC+OSIRIS	R1000B/R	3640–9390	7
20150830	+29	TNG+LRS	LRB	3300–8080	11.0
20150907	+37	Ekar182+AFOSC	gm4/VPH6	3500–9300	14
20150927	+56	GTC+OSIRIS	R1000B/R	3640–10390	7
20151014	+72	TNG+LRS	LRB/R	3400–9640	16
20151104	+92	Ekar182+AFOSC	gm4/VPH6	3500–9300	14
20151204	+121	Ekar182+AFOSC	gm4	3460–8240	13.5
20151229	+146	NOT+ALFOSC	gm4	3350–9070	18
20160208	+184	GTC+OSIRIS	R1000B/R	3630–10400	7
20160401	+235	GTC+OSIRIS	R1000B/R	3640–10390	7
20160526	+289	GTC+OSIRIS	R1000R	5100–10390	8

Note. The rest phases are relative to the *V*-band maximum (2015 August 1).

Table 2. *ugriz* photometry (AB system) of ASASSN-15no.

MJD	rest phase	*u*(err)	*g*(err)	*r*(err)	*i*(err)	*z*(err)	Instrument
57240.96	+6	–	16.36 (0.08)	16.47 (0.06)	16.59 (0.09)	–	AFOSC
57243.93	+9	16.65 (0.02)	16.32 (0.05)	16.44 (0.06)	16.50 (0.08)	16.52 (0.04)	AFOSC
57244.93	+10	16.62 (0.05)	16.43 (0.04)	16.48 (0.06)	16.58 (0.06)	16.62 (0.03)	AFOSC
57245.92	+11	16.69 (0.05)	16.38 (0.05)	16.48 (0.06)	16.63 (0.10)	16.63 (0.06)	AFOSC
57258.97	+23	17.28 (0.03)	16.75 (0.05)	16.63 (0.04)	16.71 (0.04)	16.70 (0.04)	ALFOSC-FASU
57263.91	+28	–	–	16.84 (0.19)	–	–	OSIRIS
57272.89	+37	17.50 (0.07)	17.01 (0.07)	16.93 (0.04)	17.00 (0.08)	16.78 (0.05)	AFOSC
57292.86	+56	–	–	17.18 (0.01)	–	–	OSIRIS
57309.87	+72	17.91 (0.06)	17.54 (0.06)	17.45 (0.07)	17.45 (0.05)	–	LRS
57330.79	+92	18.12 (0.09)	17.74 (0.07)	17.54 (0.06)	17.77 (0.10)	17.27 (0.04)	AFOSC
57342.71	+104	–	17.89 (0.20)	17.93 (0.08)	18.07 (0.11)	17.70 (0.06)	AFOSC
57359.22	+120	19.16 (0.17)	18.34 (0.07)	18.09 (0.06)	18.26 (0.07)	18.14 (0.05)	AFOSC
57386.22	+146	19.89 (0.14)	18.88 (0.07)	18.56 (0.06)	18.74 (0.05)	18.57 (0.07)	ALFOSC-FASU
57426.23	+185	–	–	19.84 (0.03)	–	–	OSIRIS
57429.19	+187	>20.66 (0.36)	20.09 (0.11)	19.91 (0.11)	20.13 (0.19)	19.37 (0.09)	AFOSC
57464.19	+221	>21.48 (0.51)	21.08 (0.15)	20.70 (0.13)	20.95 (0.20)	20.03 (0.20)	LRS
57479.18	+236	–	–	20.89 (0.50)	–	–	OSIRIS
57488.02	+244	–	21.48 (0.06)	21.06 (0.10)	21.23 (0.08)	–	LRS
57534.06	+289	–	–	21.59 (0.66)	21.53 (0.70)	21.17 (0.70)	OSIRIS*

Note. *i and z measurements synthesized from the spectrum after normalizing it to the r photometric measurement. The rest phases are relative to the *V*-band maximum (2015 August 1).

to infer that the rise time, in this photometric band, could have been relatively short.

The u to z light curves have very similar shapes, showing relatively fast declines from the peaks lasting about 20–40 d (we do not have a dense temporal coverage of this phase). Later on, the light curves settle on a slower linear decline up to about 100 d after maximum, with rates only mildly depending on the pass-band (e.g. 1.15 ± 0.06 mag $(100\mathrm{d})^{-1}$ in u; 1.24 ± 0.14 mag $(100\mathrm{d})^{-1}$ in r; and 0.75 ± 0.04 mag $(100\mathrm{d})^{-1}$ in z). After 100 d, all light curves show a more rapid decline rate especially in blue bands (e.g. >2.41 mag $(100\mathrm{d})^{-1}$ in u; 2.30 ± 0.08 mag $(100\mathrm{d})^{-1}$ in r; and 1.98 ± 0.10 mag $(100\mathrm{d})^{-1}$ in z). The latest r, i, and z points at $\sim$300 d suggest a possible flattening, but the large uncertainties in the measurements prevent us from a robust statement.

4 SPECTROSCOPIC ANALYSIS

The journal of the spectroscopic observations is reported in Table 1, along with the information on the instrumental configurations used and spectral resolutions. The results of the spectroscopic follow-up campaign of ASASSN-15noare shown in Fig. 2. The spectra are shown in the observer's frame and are not corrected for the Galactic extinction.

The spectra at early phases are characterized by a blue continuum. The temperature (estimated through a blackbody fit) is initially

Table 3. *UBVRI* photometry (Vega system) of ASASSN-15no.

MJD	rest phase	*U*(err)	*B*(err)	*V*(err)	*R*(err)	*I*(err)	Instrument
57233.31	−2	–	–	>17.10	–	–	ASASSN
57237.26	+2	–	–	16.46(0.09)	–	–	ASASSN
57241.24	+6	–	–	16.50(0.13)	–	–	ASASSN
57242.28	+7	–	–	16.62(0.09)	–	–	ASASSN
57243.93	+9	–	16.55 (0.05)	16.47 (0.05)	–	–	AFOSC
57244.28	+9	–	–	16.57(0.08)	–	–	ASASSN
57244.92	+10	–	16.55 (0.06)	16.54 (0.04)	–	–	AFOSC
57245.92	+11	–	16.70 (0.08)	16.50 (0.05)	–	–	AFOSC
57246.26	+11	–	–	16.79(0.10)	–	–	ASASSN
57250.26	+15	–	–	16.68(0.09)	–	–	ASASSN
57255.25	+20	–	–	16.68(0.10)	–	–	ASASSN
57258.96	+23	–	17.01 (0.03)	16.69 (0.03)	–	–	ALFOSC-FASU
57316.80	+79	17.17 (0.11)	17.65 (0.07)	17.49 (0.06)	17.22 (0.06)	16.95 (0.05)	MEIA2
57317.80	+80	17.20 (0.12)	17.71 (0.09)	17.44 (0.05)	17.36 (0.06)	16.99 (0.07)	MEIA2
57330.79	+92	–	17.92 (0.06)	17.63 (0.04)	–	–	AFOSC
57342.71	+104	–	18.19 (0.09)	17.92 (0.09)	–	–	AFOSC
57359.23	+120	–	18.57 (0.10)	18.20 (0.05)	–	–	AFOSC
57386.21	+146	–	19.05 (0.07)	18.80 (0.07)	–	–	ALFOSC-FASU
57429.20	+187	–	20.10 (0.15)	19.88 (0.19)	–	–	AFOSC
57488.04	+244	–	21.76 (0.18)	21.38 (0.19)	–	–	LRS

Note. The rest phases are relative to the *V*-band maximum (2015 August 1).

very high, 13 300 ± 300 K at +6 d, rapidly drop to 8200 ± 300 K at +23 d, and stays nearly constant hereafter (see Section 6.1). The first feature clearly seen in the spectra beginning at +11 d onwards is a line with a broad and shallow P-Cygni profile probably due to He I 5876 Å. The expansion velocity deduced from the minimum of its absorption is about 8700 km s^{-1}. At the same time a broad (FWHM ∼ 8000 km s^{-1}) Hαemission begins to grow. On day +37, the spectrum starts to show a growing blue continuum component blue-ward of ∼5600 Å, which increases with time. This blue pseudo-continuum is often seen in interacting SNe (Turatto et al. 1993; Smith et al. 2009) and is due to the blending of Fe line emissions. By day +56, the spectrum shows very broad H$\alpha$and Ca II-IR emissions. The Hαprofile is complex, consisting of a broad base with a half width at zero intensity of ∼23000 km s^{-1}for the blue wing and ∼13000 km s^{-1}for the red wing. An intermediate (FWHM ∼ 12000 km s^{-1}) component, blue-shifted by ∼− 2000 km s^{-1}with respect to the Hαrest frame wavelength, is superimposed to the broad emission. Starting from day +72, a broad Hβabsorption begins to appear and by day +92 an expansion velocity of about 7400 km s^{-1}is derived from its minimum.

The Ca II-IR emission has instead a triangular shape, with a FWHM ∼ 15400 km s^{-1}centred at almost its rest-frame position (see Fig. 2). This feature remains visible until late phases, with an almost constant full width at half-maximum (FWHM). However, in the last two spectra, the FWHM decreases to ∼13700 km s^{-1}at day +235, and ∼11800 km s^{-1}at day +289, caused by a fading of the red wing, and a simultaneous blueshift of the whole emission by ∼70 Å. This could be an indication of dust formation in the shocked ejecta. Hαshows a constant profile until +146 d after maximum, and then fades. In the last three spectra, it appears as a relatively faint, broad, and boxy emission blended with a now dominant [OI] doublet. The last spectra are reminiscent of those of some SE SNe, although contaminated by narrow emissions of the parent galaxy, (see Section 6.3). Besides the broad, shallow emissions, the spectra later than ∼+ 50 d show a persistent blue pseudo-continuum, typically seen in interacting SNe.

5 ABSOLUTE MAGNITUDES AND BOLOMETRIC LIGHT CURVE OF ASASSN-15no

With the values adopted for distance and extinction in Section 1 (using the Cardelli et al. 1989, extinction law), we obtain $M_V \sim -19.6 \pm 0.3$ mag at maximum light. Similar magnitudes are inferred for the *r* and *B* bands at maximum. These values are similar to those derived for some interacting SNe, such as SN 1997cy (Turatto et al. 2000) and SN 1999E (Rigon et al. 2003).

The pseudo-bolometric light curve of ASASSN-15nohas been computed by integrating its multicolour *uBgVriz* photometry, neglecting any possible contribution in other spectral ranges. The ultraviolet contribution, however, is expected to be significant especially at early stages. For each epoch and filter, we derived the flux at the effective wavelength. We adopted as reference the epochs of the *r*-band measurements (except for the first two epochs, for which we used the *V* band as reference). Missing fluxes in other filters were estimated through interpolation or, if necessary, by extrapolation from the closest available epoch assuming a constant colour with respect to adjacent bands. The flux measurements for all filters, corrected for extinction, give the spectral energy distribution at each epoch, which is integrated with the trapezoidal rule, assuming zero flux at the integration limits. The observed flux was then converted into luminosity. The resulting pseudo-bolometric light curve is shown in Fig. 3 (upper panel), along with those of a sample of SNe that includes SNe IIn with similar luminosity and spectral evolutions, the peculiar Type II SN 2009kf, and a few SE SNe, because of the similarity of the late time spectra of ASASSN-15nowith this SN type (see Section 6.3).

A 'true' bolometric light curve is also reported in Fig. 3. To construct it, we had to estimate the bolometric correction for each phase. This was performed by fitting with a blackbody the *BgVriz* spectral energy distribution (SED; we did not consider the *u* band because of the heavy line blanketing affecting this spectral region) derived in epochs where the SN had multiband detections, and then adding the missing flux, measured from 0 to ∞, to the optical

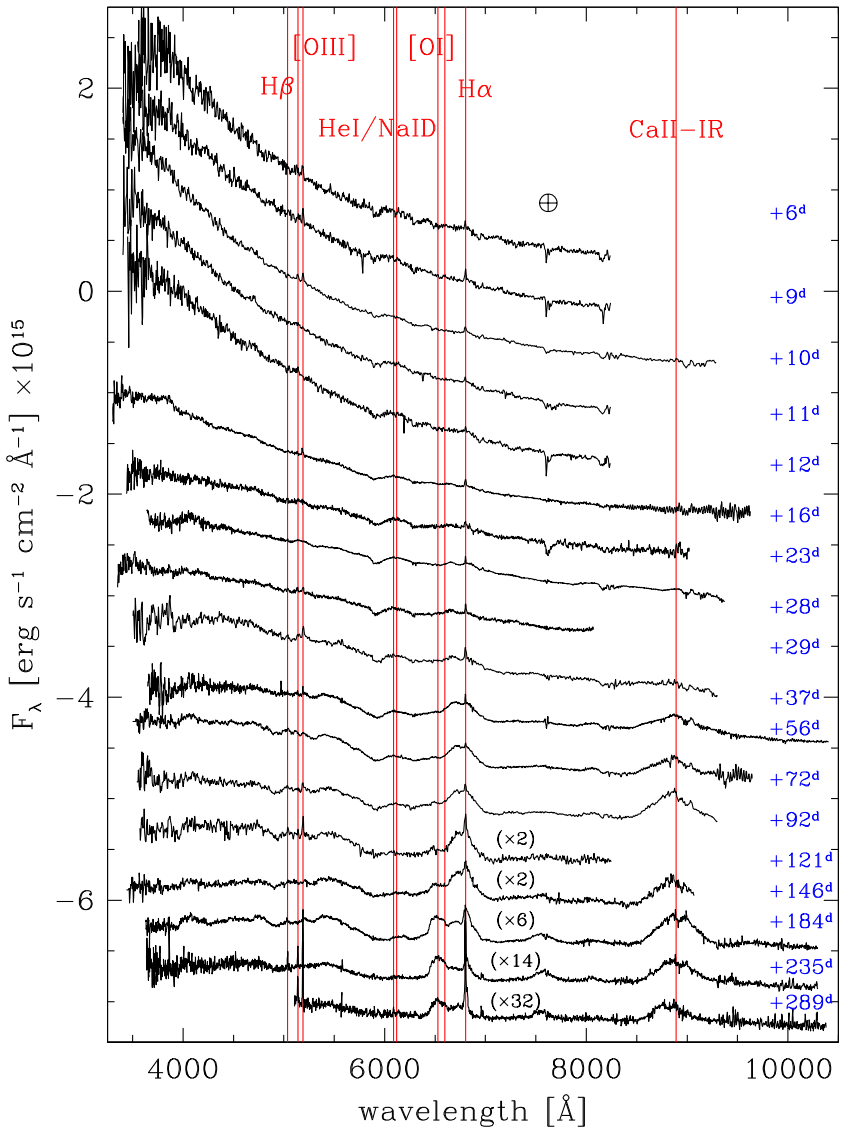

Figure 2. Spectroscopic evolution of ASASSN-15no. The wavelength scale is set in the observer's frame and is not corrected for the Galactic extinction. The ordinate refers to the first spectrum, and the others have been arbitrarily shifted downwards. For the sake of clarity, the flux counts in the last five spectra have been multiplied by the numbers given in parenthesis. Residuals from the atmospheric absorption corrections have been marked with the ⊕ symbol.

luminosities. We remark that the BB temperatures derived from the photometric SED are in close agreement with those derived from the spectral fitting (see Section 6.1). Because of the blue pseudo continuum seen in later time spectra of ASASSN-15nodue to ongoing interaction, the blackbody fit of the SED could led to an incorrect estimation of the temperature and accordingly to an overestimation of the bolometric correction. The 'true' bolometric luminosity is used for the modelling discussed in Section 6.2.

The luminosity of ASASSN-15nois intermediate between those of the Type IIn SNe 2005gj, 1997cy, and 1999E,[2] and a few dex higher than that of the energetic SE SN 1998bw. The pseudo bolometric light curve shows a regular decline from the peak to ∼40 d after maximum, followed by a slightly flatter decline up to about +100 d, similar to the comparison Type IIn SNe and SN 2009kf. However, from $\gtrsim$ 40 d onwards ASASSN-15noshows a luminosity excess with respect to SN 2009kf. After $\gtrsim$ +100 d, the decline rate of ASASSN-15noincreases again.

6 DISCUSSION

6.1 Photospheric temperature and radius evolution

The photometric and spectroscopic monitoring of the optical transient ASASSN-15nocan be used to derive some physical properties of the transient, such as the evolution of the photospheric radius and temperature. We performed a blackbody fit to our early time

[2] These three SNe share similarities with the so-called Type Ia-CSM events. A prototypical event of this class is PTF11kx, which is believed to be a thermonuclear explosion in a H-rich CSM (Dilday et al. 2012), but other events were proposed to belong to this group, including SNe 2002ic, 2005gj, and 2012ca (Hamuy et al. 2003; Prieto et al. 2007; Fox et al. 2015). We remark, however, that other authors suggested an alternative scenario with an energetic CC engine for these transients (Benetti et al. 2006; Trundle et al. 2008; Inserra et al. 2016).

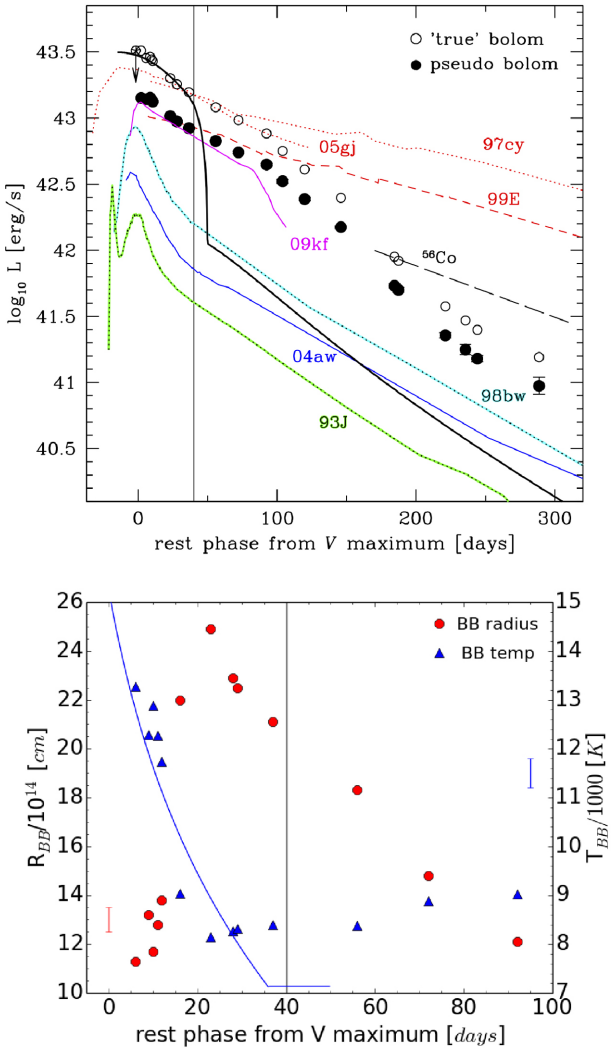

Figure 3. Top panel: comparison of the pseudo-bolometric *uBgVriz* light curve of ASASSN-15no(filled black circles), with those of a sample composed by some Type II and Type Ic SNe (integrated over the same wavelength range). The comparison sample includes (in order from high to low luminosities): SNe 2005gj (IIn, Prieto et al. 2005; Aldering et al. 2006); 1997cy (IIn, Turatto et al. 2000); 2009kf (II, Botticella et al. 2010); 1999E (IIn, Rigon et al. 2003); 1998bw (BL-Ic, Patat et al. 2001, and references therein); 2004aw (Ic, Taubenberger et al. 2006), where the higher reddening discussed in Benetti et al. (2006) has been adopted; and 1993J (IIb, Barbon et al. 1995, and references therein). The estimated full bolometric light curve of ASASSN-15no, marked with open circles is also included. The initial limit of this curve (open-skeletal symbol) was calculated from the *V*-band limit (see Table 3) and an assumed temperature of 16 200 K, as deduced from hydrodynamical modelling (cf. Section 6.2 and bottom panel). The black solid line is the bolometric curve of the best-fitting model (see the text for further details). The light vertical line marks the onset of the ejecta-CSM interaction (phase $\sim+$ 40 d). For completeness the ^{56}Co decay slope is also indicated dashed line). Bottom panel: ASASSN-15no: evolution of the blackbody radius and the temperature. The average temperature error bar of $\pm$300 K is shown on the right-hand side, while the mean error bar for the radius ($\pm0.4 \times 10^{14}$ cm) is shown on the left-hand side. The blue solid line is the photospheric temperature evolution of the best-fitting model (see the text for further details). The black vertical line marks the onset of the ejecta-CSM interaction (phase $\sim+$ 40 d).

spectra (phase $<+100$ d), after correcting for the adopted reddening and redshift values (see Section 1). The fits were done selecting the portions of the spectra free of emissions. The fit errors, depend on a number of parameters (including the wavelength extension of the spectra, the line contamination, the uncertainty in the flux calibration, and the assumed extinction) and have been estimated to be of the order of 300 K. The temporal evolution of the temperature is shown in Fig. 3, bottom panel (blue triangles). Adopting the true-bolometric light curve of Fig. 3 (upper panel), spherical symmetry and a filling factor of 1, we calculated the evolution of the blackbody radius (bottom panel in Fig. 3), up to 100 d past *V* maximum.

The photosphere around maximum is hot, with $T_{BB} \sim 13\,300$ K, then shows a steep decrease to about 8200 K at a phase of +25 d. Hereafter, until day +56, the temperature remains constant, but then it smoothly increases up to 9000 K. The late temperature behaviour (later than day $\sim+$ 40) is likely an artefact due to the contamination on the blue region of the spectra that we attribute to the on-set of ejecta-CSM collision. The photospheric radius, in the same time interval, steeply increases from 8×10^{14} cm to about 18×10^{14} cm (at a phase of +25 d), and then linearly decreases to about 10×10^{14} cm at about +90–+100 d (see Fig. 3, bottom). It is interesting to note that the photospheric expansion rate in the first 25 d after maximum is about 6.64×10^{13} cm d^{-1}, which corresponds to about 7700 km s^{-1}. This is very similar to the expansion velocity measured from the He I line visible in the spectra from +7 d after maximum (see Section 4). We deduce that for about 20 d the photosphere was locked to the same layer in the expanding ejecta, because the ejecta are highly ionized and thus opaque, and only after 20 d when the temperature is low enough to start the recombination the photosphere moves inwards in mass coordinate.

6.2 Modelling of the light curve

In order to better understand the early phases of the supernova and retrieve information about the physical properties of its progenitor at explosion, we compared the true-bolometric curve of ASASSN-15no with that predicted by the simulations described in Zampieri et al. (2003) and Zampieri (2007). This code solves the energy balance equation for ejecta of constant density in homologous expansion and yields the best-fitting model by simultaneously comparing the computed bolometric light curve, photospheric gas velocity, and temperature with the corresponding observed quantities. Although it is less accurate than a full radiative-hydrodynamic treatment (see e.g. Pumo & Zampieri 2011, 2013), it is able to provide reliable estimates of the physical conditions of the ejected gas and has been successfully applied to a number of SNe II (either to directly model the SN ejecta or to constrain the parameter space for fully hydrodynamic calculations; see e.g. Zampieri et al. 2003; Pumo et al. 2017; Zampieri 2017, and references therein). The early photospheric temperature evolution (lower panel of Fig. 3) is well fitted during the first 40 d past maximum by the model assuming that the first energy input occurred 15 d before maximum light (with an uncertainty of about 5 d, found analysing the quality of the model best fits), and the early photospheric gas velocity is constant at a value close to 6300 km s^{-1}. This is 2000 km s^{-1}lower than the expansion velocity deduced from the minimum of the He I 5876 Åtransition seen in ASASSN-15nospectra ($<v_{HeI}> =8400 \pm 500$ km s^{-1}for phases $<+75$ d), and after applying a v(Fe II 5169 Å)/v(He I 5876 Å) correction derived from SN 1993J spectra, a prototype of a SE supernova. In fact, the photospheric velocity is usually best traced using

Fe and/or Sc lines (Zampieri et al. 2003; Pumo & Zampieri 2011), which, however, are not evident in the ASASSN-15nospectra.

As shown in Fig. 3, the model well matches the bolometric light curve only for the first ∼40 d after the *V* maximum when the input energy is dominated by the recombination and radioactive decay. The physical parameters derived from the model are the following: mass of the ejecta, $M_{ej} = 2.6\,M_{\odot}$; initial radius of the photosphere, $R_0 = 2.1 \times 10^{14}$ cm; explosion energy, $E_{expl} = 0.8 \times 10^{51}$ erg. The ^{56}Ni mass, M_{Ni}, and recombination temperature are fixed at $0.15\,M_{\odot}$ and 6000 K, respectively. The values of these parameters are reasonable for a typical CC explosion, except for the radius. The derived radius of $\sim 3000\,R_{\odot}$ would be consistent only with a very extended supergiant star (see e.g. Levesque et al. 2005, on Galactic red supergiant stars properties).

It is reassuring to note that the initial radius deduced from the model is in agreement with the measurements from spectrophotometry (see Fig. 3, bottom panel).

The radius and, in general, the best-fitting model parameters (e.g. the low ejecta mass) are difficult to reconcile with the collapse of a single star, compared to a scenario involving a massive star in a binary (or multiple) system.

It is of interest to compare the physical parameters deduced for ASASSN-15nowith those derived for SN 2009kf (Botticella et al. 2010). In fact SN 2009kf share many physical properties (e.g. spectroscopic type, peak luminosity, early photometric evolution) with ASASSN-15no. Modelling the physical parameters of SN 2009kf, Utrobin et al. (2010) found a somewhat lower initial radius ($2000\,R_{\odot}$), but a much higher ejecta mass ($28.1\,M_{\odot}$), explosion energy (22 foe), and ^{56}Ni mass ($0.4\ M_{\odot}$). The differences regarding ejecta mass and total energy are understood considering that in SN 2009kf the photospheric phase lasts 90 d and is only supported by the ejecta recombination and radioactive decay, while in ASASSN-15nolasts only ∼55 d according to our scenario.

6.3 Spectroscopic comparison with a sample of core collapse SNe

We already mentioned that the ASASSN-15nolight has a BB-like energy distribution at maximum, in analogy with other SNe (e.g. 2005gj and 1993J, see top panel of Fig. 4). Instead, the near-maximum spectra of energetic SNe Ic, despite being dominated by a strong continuum, show also broad Fe II and Si II features.

The temperature of the emitting photosphere reaches its minimum value, when the radius of the photosphere is maximum, then the temperature remains almost constant, while the radius steadily decreases, and the recombination front recedes inward through the ejecta. However, the late time temperature evolution could be affected by the increasing strength of the blue pseudo-continuum, probably arising from a cool dense shell, the region where the ejecta-CSM interaction take place (Smith et al. 2009).

Overall the observations suggest the following scenario. Initially ASASSN-15noejecta is in free expansion, but ∼40 d after maximum it starts to interact with a close-by CSM. This is confirmed by the spectroscopic comparison shown in the middle panel of Fig. 4, where the spectrum of ASASSN-15noshows remarkable differences when compared with that of SN 2009kf. Hαis faint and broad, while in SN 2009kf it has a P-Cygni profile typically seen in non-interacting SNe. The ASASSN-15nospectrum shows a blue pseudo-continuum typically seen in the spectra of interacting SNe. Still, the maximum expansion velocity (∼18000 km s^{-1}, assuming an average Ca II IR triplet wavelength of 8579.1 Å, Mazzali et al. 2005) derived from the broad Ca II IR features of ASASSN-15noand SN 1998bw is comparable. After +100 d, the bolometric luminosity decline becomes steeper (upper panel of Fig. 3), which probably correspond to a phase of fading interaction. If, as assumed in our modelling, the explosion of ASASSN-15nohas ejected a ^{56}Ni mass of about $0.15\,M_{\odot}$ similar to the amount of ^{56}Ni ejected in other CC SNe, by ∼+ 250 d the contribution due to interaction reaches a minimum (see Fig. 3, upper panel). By this time, the spectrum is thus a combination of the emission coming from the interaction, and the emission from the non-interacting SN. This is best seen in the bottom panel of Fig. 4, where we show the ASASSN-15nospectrum as observed and with a subtracted BB contribution (assumed coming from the interaction and estimated from the flux difference from the ASASSN-15nobolometric luminosity with respect to that of the SE SNe, see top panel of Fig. 3). The second (subtracted) spectrum shows typical nebular features of a SE SN with a weak Hα. The simultaneous presence of interaction and ejecta features in the spectra likely indicates that the CSM is clumpy, or that its geometry and/or density structure are highly asymmetric.

6.4 6300-64 Å- [O I] lines

Following Taubenberger et al. (2009), we have de-blended the [O I] 6300-64 Åand Hαlines on the last three ASASSN-15nospectra. However, in ASASSN-15nospectra, the de-blending is complicated by the presence of the broad Hα. The central position of the 6300 feature is similar to that observed in the SN Ib/c sample presented in Taubenberger et al, and it also experiences a similar red-ward shift with time shown by the SN Ib/c sample. The FWHM is large (5000–7000 km s^{-1}at +184 d, 5400–6500 km s^{-1}at +235 d, and 5100–5900 km s^{-1}at +289 d, depending from the assumed Hαwidth) and very similar to the widths shown by the [O I] 6300 Å line in the more energetic SE–SNe (see fig. 8 of Taubenberger et al. 2009).

Hα, which is blended with the [O I] doublet, has a composite profile. At +186 d, it consists of a broad (FWHM ∼ 10000 km s^{-1}) component, blue-shifted by ∼4000 km s^{-1}(similar to that observed in early spectra, see Section 4), and an intermediate one (FWHM ∼ 3800 km s^{-1}), redshifted by ∼1100 km s^{-1}. At +294 d, while the broad component does not show a clear evolution with time, the intermediate one is found almost at the rest wavelength with a FWHM ∼ 1700 km s^{-1}.

6.5 The progenitor scenario

In an attempt to address all the observed evidences, we sketch the following scenario. The SE C/O core of a massive star, undergoes a likely asymmetric (see below) explosion, which is initially masked by an opaque H-poor/He-rich, detached shell having an inner radius of $\sim 3000\,R_{\odot}$.

Such a shell could have been lost by the SN progenitor during a common-envelope mass-loss episode with a companion star, although the uncertainties on the common-envelope evolution prevent us from having precise information on this type of episodes (see e.g. Ivanova et al. 2013; Tauris et al. 2017, and references therein).

Assuming an average expansion velocity of ∼15000 km s^{-1}for the ejecta and the initial radius deduced from the modelling ($\sim 3000\,R_{\odot}$), we can estimate that the ejecta travelled about 1.7 d before hitting the shell (likely expanding at low velocity, $\lesssim$ 100 km s^{-1}). When the outer ejecta collide with the shell, a fraction of the kinetic energy of the ejecta heats the gas, and speeds up the shell itself. If the velocity deduced from the expanding photospheric radius (7700 km s^{-1}cf. Section 5) is in fact an indication that the

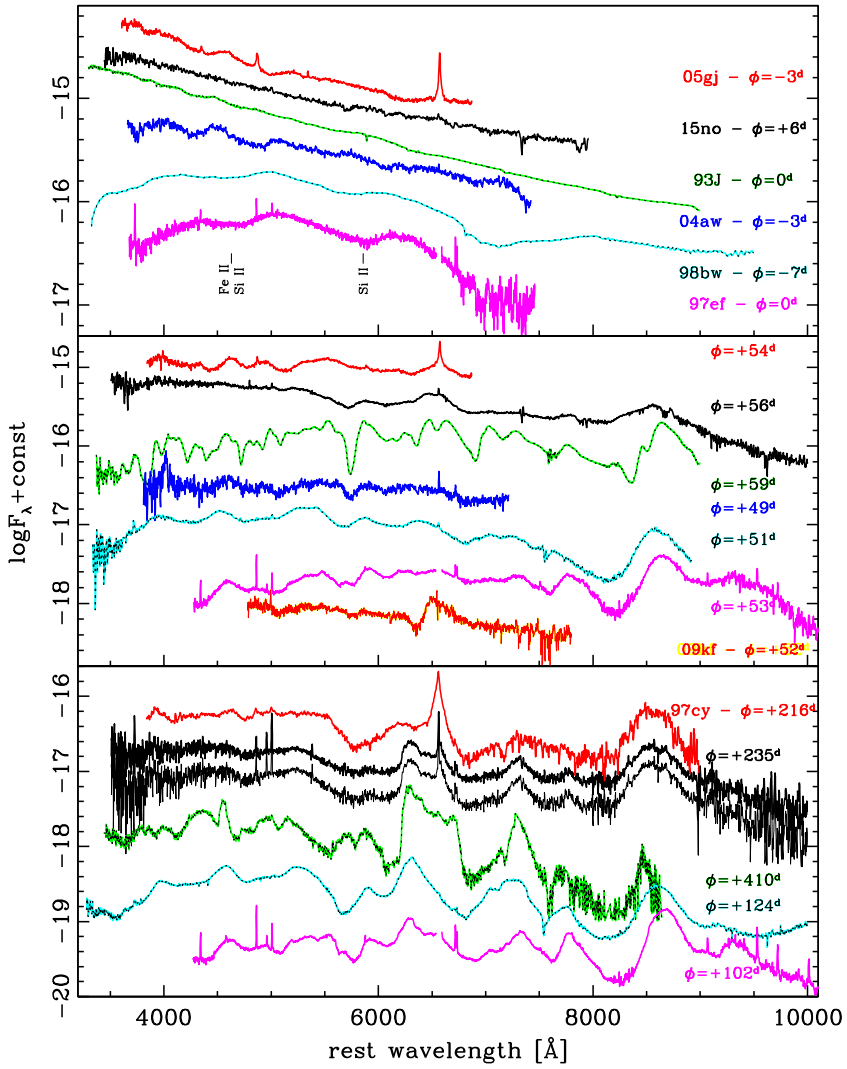

Figure 4. Comparison of ASASSN-15nospectra at three key phases with those of reference objects. In the top panel (from top): SN 2005gj (IIn, Prieto et al. 2005; Aldering et al. 2006), ASASSN-15no, SNe 1993J (IIb, Barbon et al. 1995, and references therein), 2004aw (Ic, Taubenberger et al. 2006; Modjaz et al. 2014), 1998bw (BL-Ic, Patat et al. 2001), and 1997ef (BL-Ic, Iwamoto et al. 2000). The main Si II (6355 Ådoublet and 5058 Å), and Fe II (4924, 5018, 5169, Å) absorption blends normally seen in Type Ic SNe are marked (e.g. Mazzali et al. 2000). In the middle panel, a +52 d spectrum of SN 2009kf (II, Botticella et al. 2010) has been also included. In the bottom panel, SN 2005gj is replaced by SN 1997cy (IIn, Turatto et al. 2000). In this panel, the ASASSN-15nospectrum is shown as observed (solid line) and with a BB continuum subtracted (lighter, lower line; see the text for details).

ejecta plus swept-up shell is expanding with that velocity, this is about half of the velocity of the SN ejecta alone.

Assuming that the explosion of ASASSN-15nowas similar to that of SN 1993J, whose observables were well fitted by models of Woosley et al. (1994) and Blinnikov et al. (1998), with ejected mass as low as 1.54 $M_\odot$ (assuming binarity and the formation of a remnant of 1.55 $M_\odot$) we can estimate that the mass of CSM shell enclosing the ASASSN-15noprogenitor was as high as 1 $M_\odot$(from our modelling the mass of the SN ejecta plus swept-up up material is 2.6 $M_\odot$, see Section 6.2).

This scenario involving the ejecta-shell collision could be a scaled down (both in mass and radius of the shell) version of those proposed as a possible explanation for some SLSNe-II. As an example, in the H-rich SLSN CSS121015:004244+132827 (Benetti et al. 2014), the initial radius has been estimated to be $\lesssim 2 \times 10^{15}$ cm and the shell mass to be ∼8.5 $M_\odot$, making this SLSN at least 1.0 dex more luminous than ASASSN-15no.

The ejecta plus swept-up shell material begin a mild interaction with an outer CSM about 40 d after maximum. This outer CSM has probably high density and is H-poor. We get to these conclusions because in the early spectra there is no sign of low velocity Balmer recombination lines. The faint narrow Hαline seen in early spectra mostly comes from an underlying H-II region, which contaminates the spectra at all phases (see also the presence of the [S II] doublet in the last two spectra of Fig. 2). We can use simple arguments to constraint the geometry of the system. Assuming a velocity of ∼10–100 km $s^{-1}$for the CS shell, and an initial radius of the massive shell of $R_0^{sh} = 2.1 \times 10^{14}$ cm, as suggested by the modelling, the inner shell must have been lost by the progenitor star ∼7–0.7 yr before the explosion. We can also compute when the outer CSM has been expelled by the progenitor through the formula

$t_0 = [R_0^{sh} + (v_{sh} - v_{CSM}) \times t_{int}]/v_{CSM}$,

where $R_0^{sh} = 2.1 \times 10^{14}$ cm is the initial radius of the inner shell, $v_{sh} = 6300$ km $s^{-1}$is the photospheric expansion velocity of the

swept-up shell+ejecta, $v_{CSM} = 10$–$100\,km\ s^{-1}$is the assumed expansion for the CSM (similar to the expansion velocity of the massive shell before the collision with the ejecta), $t_{int} = 50$ d is the time after which the swept-up shell+ejecta starts to interact with the CSM (taking as reference the time of the first contact of the ejecta with the shell). The result is that the outer CSM has been lost by the progenitor star about 90–9 yr before the SN explosion.

At phases later than +100 d, the CSM surrounding the SN is almost swept-up and the radiation is coming from the inner part of the SN ejecta, however, as seen from the presence of the intermediate-width Hα, some residual CSM interaction is still ongoing.

Because of the pronounced blueshift of the broad Hαemission seen at all phases, we suggest that the SN ejecta are asymmetric, with the asymmetric axes pointing in the observer's direction.

In summary, we propose that what we initially observe in ASASSN-15nois the result of the collision between the SN ejecta (not visible early on) with a pre-existing, massive shell. Since the late time spectra turn out to be very similar to the nebular spectra of SE-SN, we propose that the shell could be the result of mass-loss due to a common-envelope phase in a binary system. This is in fact the favoured channel proposed for stripping the external H-He mantle of massive stars before their explosion as SE SNe (Podsiadlowski et al. 1992; Yoon et al. 2010; Eldridge et al. 2013). In binary systems, the SN progenitors may also be surrounded by dense CSM because of the mass loss triggered by non-conservative mass transfer along the final phases of the progenitor evolution (Ouchi & Maeda 2017).

Alternatively, a massive binary system composed by a H-poor LBV-like star that expelled a shell ∼7–0.7 yr before a Wolf–Rayet companion star exploded as ASASSN-15no, could also explain the observations. A similar progenitor configuration has been proposed by Pastorello et al. (2007) to explain the output of the type Ibn SN 2006jc (however, this scenario has been questioned by Maund et al. 2016).

7 CONCLUSIONS

Extensive photometric and spectroscopic observations of ASASSN-15nofor slightly less than a year of its evolution are presented. The light curve show a slow evolution early on, which is followed by a faster evolution 100 d after maximum, with the *V* light curve reaching an absolute magnitude peak of $M_V \sim -19.6$.

The spectra up to ∼10 d after maximum are featureless with BB temperature dropping from 13 300 K at maximum to 8200 K 17 d later. At phase of +11 d, a He I 5876 Åtransition with a P-Cygni profile appears, with an expansion velocity of about 8000 km s^{-1}. At phases later than +40 d from the *V* maximum, the blue region of the spectra are dominated by a blue pseudo-continuum frequently seen in interacting SNe. Meanwhile, a broad Hαbecomes more and more intense with time up to ∼150 d after the *V*-band maximum and quickly declines later on. At the same phases an intermediate Hαcomponent appears, which becomes narrower and fainter with time. The spectra at latest phases look very similar to the nebular spectra of SE SNe.

The early photometric evolution (the first 40 d after the *V* maximum) of the bolometric light curve is well reproduced by a model in which the post-explosive evolution is dominated by the expanding ejecta and the energy budget is essentially coming from ejecta recombination and ^{56}Ni decay. From this we infer, a mass of the ejecta, $M_{ej} = 2.6\,M_{\odot}$; an initial radius of the photosphere, $R_0 = 2.1 \times 10^{14}$ cm; and an explosion energy, $E_{expl} = 0.8$ foe. The blue pseudo-continuum and the intermediate Hαcomponent are, instead, clues that ejecta-CSM interaction starts from about 40 d after maximum.

A possible scenario that accounts for all the observables involves a massive and extended H-poor shell lost by the progenitor star (1–7 yr before explosion), probably during a common-envelope episode with a companion. The shell is heated and accelerated by the collision with the ejecta and its emission models the early bolometric light curve. The accelerated shell+ejecta rapidly dilutes unveiling the unperturbed supernova spectrum below. Meanwhile, the shell+ejecta start to interacts with a more H-poor external circumstellar material lost by the progenitor system about 9–90 yr before the explosion. This interaction should occur in clumps or in highly asymmetric CSM, because only in this scenario, the inner ejecta are exposed.

This scenario involving the ejecta-massive shell collision could be a scaled down (both in mass and radius of the shell) version of those proposed for modelling some SLSNe.

ACKNOWLEDGEMENTS

We thank the ASAS-SN team for providing their photometry for ASASSN-15no. We also thank the anonymous referee for helpful comments. SB, AP, NE-R, GT, MT, and LT are partially supported by the PRIN-INAF 2014 (project 'Transient Universe: unveiling new types of stellar explosions with PESSTO'). ST acknowledges support by TRR 33 'The Dark Universe' of the German Research Foundation (DFG). Based on observations made with: The Cima Ekar 1.82 m Telescopio Copernico of the Istituto Nazionale di Astrofisica of Padova, Italy. The Gran Telescopio Canarias (GTC) operated on the island of La Palma at the Spanish Observatorio del Roque de los Muchachos of the Instituto de Astrofisica de Canarias. The Nordic Optical Telescope (NOT), operated by the NOT Scientific Association at the Spanish Observatorio del Roque de los Muchachos of the Instituto de Astrofisica de Canarias. The Italian Telescopio Nazionale Galileo (TNG) operated on the island of La Palma by the Fundación Galileo Galilei of the INAF (Istituto Nazionale di Astrofisica) at the Spanish Observatorio del Roque de los Muchachos of the Instituto de Astrofisica de Canarias. The Telescopi Joan Orò of the Montsec Astronomical Observatory, which is owned by the Generalitat de Catalunya and operated by the Institute for Space Studies of Catalunya (IEEC). This work has made use of the NASA/IPAC Extragalactic Database (NED), which is operated by the Jet Propulsion Laboratory, California Institute of Technology, under contract with NASA. We also used NASA's Astrophysics Data System.

Funding for SDSS-III has been provided by the Alfred P. Sloan Foundation, the Participating Institutions, the National Science Foundation, and the U.S. Department of Energy Office of Science. The SDSS-III web site is http://www.sdss3.org/. SDSS-III is managed by the Astrophysical Research Consortium for the Participating Institutions of the SDSS-III Collaboration including the University of Arizona, the Brazilian Participation Group, Brookhaven National Laboratory, Carnegie Mellon University, University of Florida, the French Participation Group, the German Participation Group, Harvard University, the Instituto de Astrofisica de Canarias, the Michigan State/Notre Dame/JINA Participation Group, Johns Hopkins University, Lawrence Berkeley National Laboratory, Max Planck Institute for Astrophysics, Max Planck Institute for Extraterrestrial Physics, New Mexico State University, New York University, Ohio State University, Pennsylvania State University, University of Portsmouth, Princeton University, the Spanish Participation

Group, University of Tokyo, University of Utah, Vanderbilt University, University of Virginia, University of Washington, and Yale University.

REFERENCES

Adams S. M., Kochanek C. S., Gerke J. R., Stanek K. Z., 2016, MNRAS, 469, 1445
Ahn C. P. et al., 2012, ApJS, 203, 21
Ahn C. P. et al., 2014, ApJS, 211, 17
Aldering G. et al., 2006, ApJ, 650, 510
Balam D. D., Graham M. L., 2015, Astron. Telegram, 7931
Barbon R. et al., 1995, A&AS, 110, 513
Benetti S., Cappellaro E., Turatto M., Taubenberger S., Harutyunyan A., Valenti S., 2006, ApJ, 653, L129
Benetti S. et al., 2014, MNRAS, 441, 289
Blinnikov S. I., Sorokina E. I., 2010, preprint (arXiv:1009.4353)
Blinnikov S. I., Eastman R., Bartunov O. S., Popolitov V. A., Woosley S. E., 1998, ApJ, 496, 454
Botticella M. T. et al., 2009, MNRAS, 398, 1041
Botticella M. T. et al., 2010, ApJ, 717, L52
Cappellaro E., 2014, SNOoPy: a package for SN photometry, available at http://sngroup.oapd.inaf.it/snoopy.html
Cardelli J. A., Clayton G. C. Mathis J. S., 1989, ApJ, 345, 245
Chevalier R. A., Irwin C. M., 2011, ApJ, 729, L6
Chonis T. S., Gaskell C. M., 2008, AJ, 135, 264
Dexter J., Kasen D., 2013, ApJ, 772, 30
Dilday B. et al., 2012, Science, 337, 942
Dong S. et al., 2016, Science, 351, 257
Eldridge J. J., Fraser M., Smartt S. J., Maund J. R., Crockett R. M., 2013, MNRAS, 436, 774
Filippenko A. V., 1997, ARA&A, 35, 309
Fox O. D. et al., 2015, MNRAS, 447, 772
Gal-Yam A., 2012, Science, 337, 927
Gal-Yam A. et al., 2009, Nature, 462, 624
Hamuy M. et al., 2003, Nature, 424, 651
Heger A., Fryer C. L., Woosley S. E., Langer N., Hartmann D. H., 2003, ApJ, 591, 288
Holoien T. W.-S. et al., 2015, Astron. Telegram, 7869
Holoien T. W.-S. et al., 2017, MNRAS, 467, 1098
Inserra C. et al., 2013, ApJ, 770, 128
Inserra C. et al., 2016, MNRAS, 459, 2721
Ivanova N. et al., 2013, A&A Rev., 21, 59
Iwamoto K. et al., 2000, ApJ, 534, 660
Kasen D., Bildsten L., 2010, ApJ, 717, 245
Kuncarayakti H. et al., 2017, ApJ, in press
Levesque E. M., Massey P., Olsen K. A. G., Plez B., Josselin E., Maeder A., Meynet G., 2005, ApJ, 628, 973
Maund J. R., Pastorello A., Mattila S., Itagaki K., Boles T., 2016, ApJ, 833, 128
Mazzali P. A., Iwamoto K., Nomoto K., 2000, ApJ, 545, 407
Mazzali P. A. et al., 2005, ApJ, 623, L37
Mazzali P. A., Walker E. S., Pian E. Tanaka M., Corsi A., Hattori T., Gal-Yam A., 2013, MNRAS, 432, 2463
Modjaz M. et al., 2014, AJ, 147, 99
Moriya T., Tominaga N., Tanaka M., Maeda K., Nomoto K., 2010, ApJ, 717, L83
Nicholl M. et al., 2013, Nature, 502, 346
Ouchi R., Maeda K., 2017, ApJ, 840, 90
Pastorello A. et al., 2004, MNRAS, 347, 74
Pastorello A. et al., 2007, Nature, 447, 829
Pastorello A. et al., 2010, ApJ, 724, L16
Pastorello A. et al., 2016, MNRAS, 456, 853
Patat F. et al., 2001, ApJ, 555, 900
Planck Collaboration XIII, 2015, A&A, 594, A13
Podsiadlowski P., Joss P. C., Hsu J. J. L., 1992, ApJ, 391, 246
Prieto J. et al., 2005, IAU Circ., 8633, 1
Prieto J. L. et al., 2007, AJ, preprint (arXiv:0706.4088)
Pumo M. L., Zampieri L., 2011, ApJ, 741, 41
Pumo M. L., Zampieri L., 2013, MNRAS, 434, 3445
Pumo M. L., Zampieri L., Spiro S., Pastorello A., Benetti S., Cappellaro E., Manic G., Turatto M., 2017, MNRAS, 464, 3013
Quimby R. M. et al., 2011, Nature, 474, 487
Reynolds T. M., Fraser M., Gilmore G., 2015, MNRAS, 453, 2885
Riess A. G. et al., 2016, ApJ, 826, 56
Rigon L. et al., 2003, MNRAS, 340, 191
Schlafly E. F., Finkbeiner D. P., 2011, ApJ, 737, 103
Schlegel E. M., 1990, MNRAS, 244, 269
Shappee B. J. et al., 2014, ApJ, 788, 48
Smith N. et al., 2009, ApJ, 695, 1334
Spiro S. et al., 2014, MNRAS, 439, 2873
Stetson P. B., 1987, PASP, 99, 191
Taubenberger S. et al., 2006, MNRAS, 371, 1459
Taubenberger S. et al., 2009, MNRAS, 397, 677
Tauris T. M. et al., 2017, ApJ, 846, 170
Terreran G. et al., 2017, Nat. Astron., 1, 713
Trundle C., Kotak R., Vink J. S., Meikle W. P. S., 2008, A&A, 483, L47
Turatto M., Benetti S., Pastorello A., 2007, in Immler S., Weiler K., eds, AIP Conf. Ser. Vol. 937, Supernova 1987A: 20 Years After: Supernovae and Gamma-Ray Bursters. Am. Inst. Phys., New York, p. 187
Turatto M. et al., 1993, MNRAS, 262, 128
Turatto M. et al., 2000, ApJ, 534, L57
Utrobin V. P., Chugai N. N., Botticella M. T., 2010, ApJ, 723, L89
Wheeler J. C., Chatzopoulos E., Vinko J., Tuminello R., 2017, ApJ, 851, L14
Whitesides L. et al., 2017, ApJ, 851, 107
Woosley S. E., 2010, ApJ, 719, L204
Woosley S. E., Eastman R. G., Weaver T. A., Pinto P. A., 1994, ApJ, 429, 30
Yoon S.-C., Woosley S. E., Langer N., 2010, ApJ, 725, 940
Young D. R. et al., 2010, A&A, 512, A70
Zampieri L., 2007, AIPC, 924, 358
Zampieri L. 2017, in Alsabti A. W., Murdin P., eds, Light Curves of Type II Supernovae chapter of Handbook of Supernovae. Springer e-book
Zampieri L. et al., 2003, MNRAS, 338, 711

This paper has been typeset from a TEX/LATEX file prepared by the author.